6.2 THE INTERACTION OF SIMULATED SQUALL LINES WITH IDEALIZED TERRAIN

Jeffrey Frame* and Paul Markowski

Department of Meteorology, Pennsylvania State University, University Park, PA

1. Introduction

The past fifty years of squall line studies have generated much understanding of these convective systems. Nearly all previous squall line studies were conducted in a manner such that the convective system was relatively free of outside influences, including those due to complex terrain. Squall lines are not only limited to regions with negligible topography, however. A review of the literature reveals one previous study (Teng et al. 2000) which examines the interaction between a pre-existing squall line and the mountainous terrain on the island of Taiwan. This investigation found that the topography retarded the speed of the gust front, allowing precipitation to fall into the inflow at the front of the system. The rear-to-front (RTF) flow was also subject to orographic ascent and became ingested into the updrafts. A combination of these factors led to the disintegration of the system as it moved up the terrain, suggesting that terrain can significantly influence quasi-linear convective systems.

In this paper, we present the results of a numerical study of squall lines traversing an idealized mountain ridge. Our simulations indicate that a squall line strengthens slightly owing to orographic ascent on the windward slopes of the ridge, weakens during descent, and then rapidly reintensifies downstream of the terrain owing to a hydraulic jump in the outflow.

The next section specifies the simulation design and model characteristics. Section 3 presents the control simulation, run with flat terrain. The mountain ridge experiment is presented in section 4. Finally, we discuss the conclusions in section 5.

2. Simulation design

The squall line simulations are performed using the Advanced Regional Prediction System (ARPS) model, version 4.5.2 (Xue et al. 1995). The model neglects radiation, surface drag, ice physics, and Coriolis effects.

The domain size is $400 \times 60 \times 17$ km. The model employs a regular grid spacing of 1.25 km in each horizontal direction. This horizontal resolution is coarser than the 100 m advocated by Bryan et al. (2003). A grid spacing on the order of 1 km, however, can resolve basic squall line structure (Bryan et al. 2003). This being a pilot study, we would rather explore a large parameter space with relatively coarse resolution than explore a smaller parameter space with higher resolution.

The vertical grid is a stretched terrain-following grid with an average spacing of 500 m and a minimum spacing of 150 m near the surface. A periodic boundary condition is imposed at the northern and southern edges of the domain. An open radiation condition is specified at the eastern and western boundaries, permitting gravity waves to propagate out of the domain. A rigid lid exists at the top of the domain with a sponge layer beneath it to absorb gravity waves (Klemp and Durran 1983).

The pre-storm environment is horizontally homogeneous and is characterized by the analytic thermodynamic profile developed by Weisman and Klemp (1982). The sounding contains 2200 J kg^{-1} of convective available potential energy (CAPE). The vertical wind profile consists of pure westerly shear, with the wind speed increasing linearly from zero at the surface to 17.5 m s^{-1} at an altitude of 2500 m. The wind velocity is constant with height above this level. This shear profile falls within the "optimal state" for squall line longevity as defined by Weisman et al. (1988). There is initially no north-south wind component.

We initiate convection with a 4.0 K warm bubble containing random perturbations of 0.1 K. The thermal has a radius of 10 km in the east-west direction, extends 3 km in the vertical direction, and is infinite in the north-south direction. It is centered at $x = 25$ km and $z = 1500$ m. This thermal generates a quasi-two-dimensional squall line, which reaches maturity after about two hours of simulation time.

In the terrain case described in detail, an idealized mountain exists at $x = 200$ km. This ridge has an east-west radius of 10 km, is infinite in the north-south direction, and has a height of 900 m. The squall line reaches the mountain just after attaining maturity. We also consider a control simulation, which is conducted with flat terrain at an elevation of 0 m.

3. Control simulation

A plot total accumulated rainfall at 18000 s (Fig. 1a) reveals significant along line structure to the squall line in the control simulation. Repeated development of heavy convective cells can be seen along $y = 15$ km from $x =$ 180 to 260 km. Other parts of that same meridional strip of the domain, however, like for $20 < y < 25$ km, and along $y = 35$ km, have total rainfall amounts less than 10 mm, suggesting a dearth of deep moist convec-

* *Corresponding author address*: Jeffrey Frame, Department of Meteorology, Pennsylvania State University, 503 Walker Building, University Park, PA 16802; *e-mail*: jwf155@psu.edu.

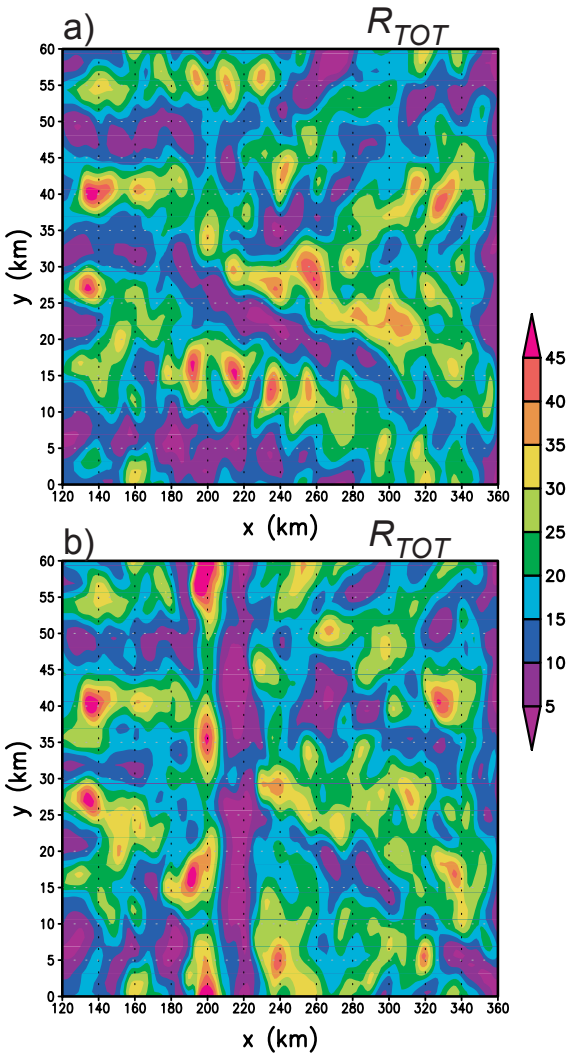

FIG. 1. Total accumulated rainfall (mm) at 18000 s for (a) the control simulation and (b) the mountain ridge simulation.

tion in those areas. Such along-line variability in three dimensional simulations of squall lines is common (e.g., Coniglio and Stensrud 2001).

Vertical cross sections taken along $y = 15$ km depict a cell life cycle similar to that seen in the simulations of Fovell and Tan (1998) and Lin and Joyce (2001). At 9300 s (Fig. 2a), an intense cell is located over $x = 185$ km, approximately 10 km behind the gust front and associated shallow updraft at $x = 195$ km. An older, decaying cell is seen to the rear of the mature cell, at $x = 177$ km. By 10500 s (Fig. 2b), the mature and decaying cells seen at 9300 s have merged, and a rather intense cell is now over $x = 210$ km, which developed from the gust front updraft (GFU) during the previous 1200 s.

Although the convection is weaker along $y = 35$ km, the cells still possess the same basic life cycle as those along $y = 15$ km (Figs. 2c, d). At 11100 s (Fig. 2d; note the different x-axis), there are no updrafts stronger than 8 m s^{-1}, which corresponds well with the precipitation minimum near $x = 240$ km, $y = 35$ km (Fig. 1a).

4. Mountain ridge simulation

The accumulated rainfall in the simulation with the mountain ridge (Fig. 1b) is quite different from that in the control simulation, especially near and just downstream from the ridge. There exists a north-south stripe of rainfall maxima approximately over the ridge, at $x = 200$ km. Just downstream from this feature, at $x = 220$ km, is an even more distinct minimum in total rainfall, also running north-south across the entire domain. Given that the total rainfall from the two simulations is nearly identical west of $x = 190$ km, and that the only difference between the two simulations is the presence of a topographical feature at $x = 200$ km in one of the simulations, then the differences cited above between the two simulations must be due to the terrain. Another north-south oriented rainfall maximum may be found at $x = 240$ km. Downstream of this feature, the line regains more along-line variability, and thus similarity with the control simulation, although the results in the eastern portion of the domain are far from identical. For example, the periodic development of intense cells along $y = 15$ km in the control simulation disappears after the squall line traverses the ridge.

A vertical cross section from the terrain run taken along $y = 15$ km at 10500 s (Fig. 3a) shows no evidence of a mature cell. A vigorous updraft is growing over the gust front at $x = 217$ km, however. This figure bares little resemblance to one taken from the same time in the control simulation (Fig. 2b). The cold pool nose is quite steep at this time, more so than in the control simulation. Such a gust front orientation is more favorable for convective initiation there (e.g., Xue et al. 1997). The cold pool becomes abruptly shallow behind the gust front (near $x = 210$ km), and this structure is indicative of a hydraulic jump. The formation mechanisms for this are discussed below.

Looking at $y = 35$ km, we see that the cell near the top of the gust front updraft (over $x = 195$ km) is stronger and deeper at the same time than in the control run (Figs. 2c and 3b). The cell just behind this one, at $x = 185$ km is weaker in the terrain simulation, likely because the stronger cell in front of it has depleted its supply of potentially warm inflow from the front of the system. At this time, the gust front is located very near the summit of the ridge. It appears that additional ascent at the gust front, due to the orography, forced a stronger updraft to grow from the GFU. The stronger updrafts found here, which are aided by orographic ascent on the windward slopes of the terrain, explain the first rainfall maximum in Fig. 1b.

At 10500 s, the vertical motion field and the cold pool at $y = 35$ km look remarkably similar to that seen at $y = 15$ km (compare Figs. 3a and 3c). This is again supported by the total rainfall pattern, which shows little variability in the y-direction just after the system passes over the topography. Also notice the lack of any mature cell at either $y = 15$ or 35 km, which is coincident with the rainfall minimum seen just east of the lee slopes of the ridge. By 11100 s, an intense cell has formed out of the GFU and is located over $x = 225$

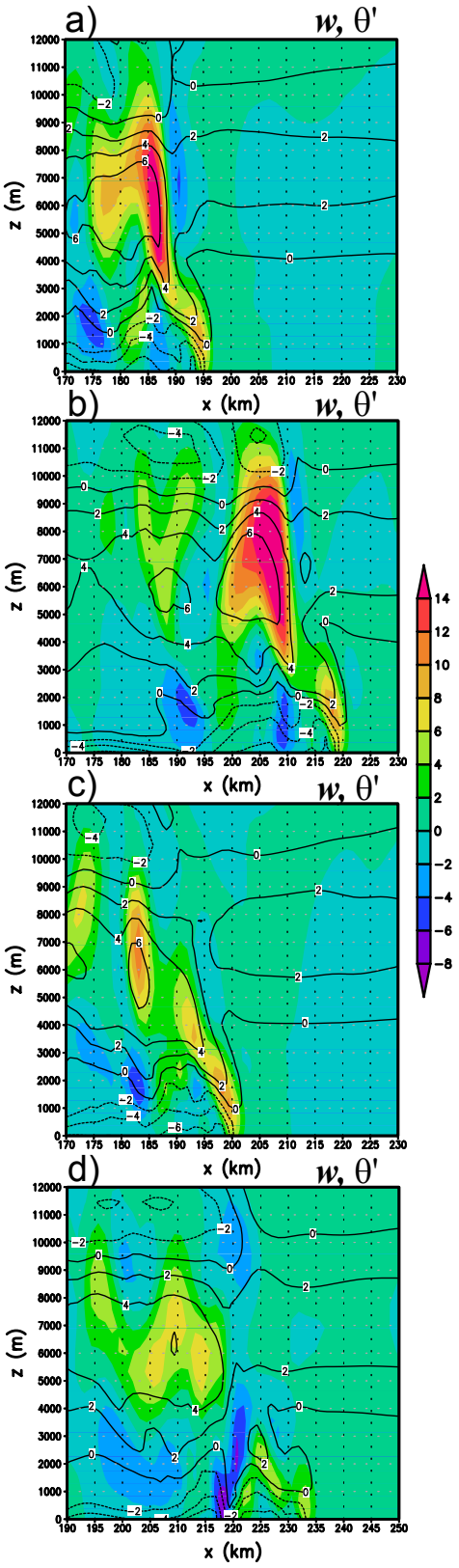

FIG. 2. Vertical cross section of vertical velocity, w, (m s^{-1}, shaded) and potential temperature perturbation, θ', (K, contoured) for the control simulation at (a) $y = 15$ km, 9300 s; (b) $y = 15$ km, 10500 s; (c) $y = 35$ km, 9600 s; and (d) $y = 35$ km, 11100 s. Note the different x-axis in (d).

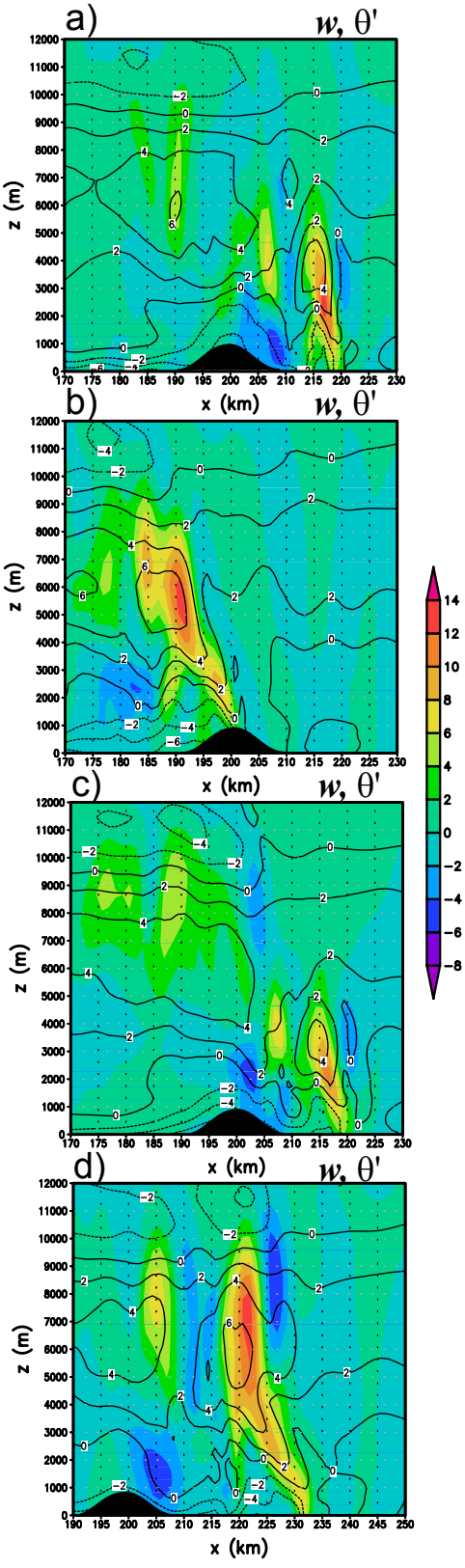

FIG. 3. Vertical cross section of vertical velocity, w, (m s^{-1}, shaded) and potential temperature perturbation, θ', (K, contoured) for the mountain ridge simulation at (a) $y = 15$ km, 10500 s; (b) $y = 35$ km, 9600 s; (c) $y = 35$ km, 10500 s; and (d) $y = 35$ km, 11100 s. Note the different x-axis in (d).

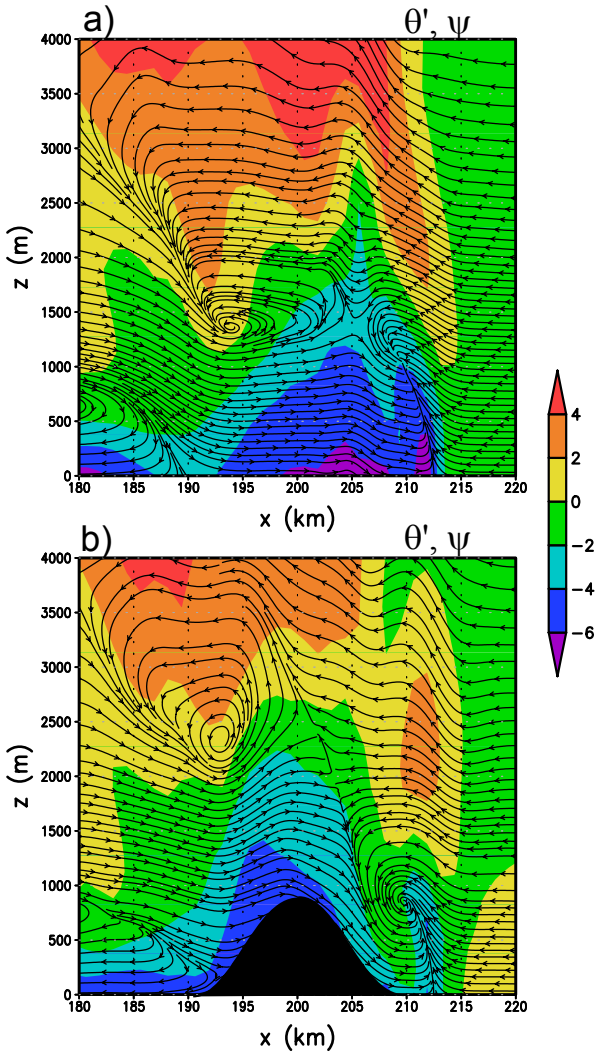

FIG. 4. System relative streamline analysis and potential temperature perturbation (shaded) at 10200 s for (a) the control simulation and (b) the mountain ridge simulation. A propagation speed of 20 m s^{-1} has been subtracted from the zonal wind component to create a storm-relative velocity profile.

km. This agrees well with the rainfall maximum seen downstream of the mountain. Thus, it after the initial orographic ascent, new cell formation is first inhibited as the system descends the terrain, then becomes favored just downstream the topography.

System-relative streamline analyses for the control and terrain runs at 10200 s are reproduced in Fig. 4. In both cases, the gust front is located at $x = 212$ km. The horizontal vorticity center seen near $x = 195$ km, $z = 1500$ m in the control simulation has been subjected to orographic ascent and is at an altitude of 2400 m in the terrain run. Also evident in the mountain ridge experiment, however, is the shallow layer of outflow descending the eastern slopes of the mountain. As the depth of the cold pool nose is reduced at the beginning of the descent, the flow in the cold pool transitions from subcritical to supercritical, as defined by the dimensionless Froude number. As the cold air accumulates at the bottom of the hill, the flow transitions back to subcritical, creating the hydraulic jump (Figs. 3a, c, and 4b). The density current head is also rather shallow during the descent, which prevents the formation of new cells at the gust front (Xue et al. 1997), explaining the lack of mature convection seen just after the system descends the ridge.

5. Final remarks

These simulations show that as a squall line impinges upon a mountain ridge, the updrafts are first intensified through orographic ascent. As the system descends the ridge, the cold pool nose becomes shallow, resulting in a minimum in convection just downwind of the topography. When the gust front reaches the bottom of the slope, a hydraulic jump forms in the outflow, forcing a steep cold pool head, which is known to be associated with increased lift at the gust front. These results have also been reproduced in preliminary simulations using 500 m horizontal grid resolution.

Considerable work remains regarding the interaction between pre-existing convection and terrain. An observational study of convection passing over complex terrain could confirm many of the conclusions reached from our idealized simulations. Also, more simulations are required to determine how environmental conditions influence the interactions reported here. Simulations using surface physics, higher grid resolution, and more realistic terrain configurations and microphysics schemes also should be attempted.

Acknowledgments. We are thankful for comments provided by Drs. Yvette Richardson and John Clark. This work was supported by a grant from the Cooperative Program for Operational Meteorology, Education and Training (COMET), Outreach Program (University Corporation for Atmospheric Research Award No. NA97WD0082), and by an American Meteorological Society graduate fellowship, sponsored by the National Weather Service.

REFERENCES

Bryan, G. H., J. C. Wyngaard, and J. M. Fritsch, 2003: Resolution requirements for the simulation of deep moist convection. *Mon. Wea. Rev*, **131**, 2394–2416.

Coniglio, M. C. and D. J. Stensrud, 2001: Simulation of a progressive derecho using composite initial conditions. *Mon. Wea. Rev.*, **129**, 1593–1616.

Fovell, R. G. and P.-H. Tan, 1998: The temporal behavior of numerically simulated multicell-type storms. Part II: The convective life cycle and cell regeneration. *Mon. Wea. Rev.*, **126**, 551–577.

Klemp, J. B. and D. R. Durran, 1983: An upper boundary condition permitting internal gravity wave radiation in numerical mesoscale models. *Mon. Wea. Rev*, **111**, 430–444.

Lin, Y.-L. and L. E. Joyce, 2001: A further study of the mechanisms of cell regeneration, propagation, and development within two-dimensional multicell storms. *J. Atmos. Sci.*, **58**, 2957–2988.

Teng, J.-H., C.-S. Chen, T.-C. C. Wang, and Y.-L. Chen, 2000: Orographic effects on a squall line system over Taiwan. *Mon. Wea. Rev.*, **128**, 1123–1138.

Weisman, M. L. and J. B. Klemp, 1982: The dependence of numerically simulated convective storms on vertical wind shear and buoyancy. *Mon. Wea. Rev.*, **110**, 504–520.

———, ———, and R. Rotunno, 1988: Structure and evolution of numerically simulated squall lines. *J. Atmos. Sci.*, **45**, 1990–2013.

Xue, M., K. K. Droegemeier, V. Wong, A. Shapiro, and K. Brewster, 1995: *ARPS Version 4.0 User's Guide.* Center for Analysis and Prediction of Storms, University of Oklahoma, 380 pp.

———, Q. Xu, and K. K. Droegemeier, 1997: A theoretical and numerical study of density currents in nonconstant shear flows. *J. Atmos. Sci.*, **54**, 1998–2019.